



Study on the estimation method for the mean stress effect on the fatigue strength of welded joints with various failure modes and joint types

Yukihide Yoshihara¹ · Naoki Osawa² · Hidekazu Murakawa³ · Peiyuan Dai²

Received: 15 September 2023 / Accepted: 21 July 2024
© The Author(s) 2024

Abstract

In compact box-shaped steel structures, partial penetration welds are frequently selected as the welding technique, and root fatigue failure might manifest in these joints. In order to ensure the structural integrity of steel structures, it is necessary to develop an assessment approach for evaluating the efficacy of post-weld heat treatment (stress relief) in enhancing the fatigue strength of root-failed welded joints. In this study, bending fatigue experiments employing stress ratios of $R=0$ and -1 have been carried out on as-welded and stress-relieved welded joint specimens. The test objects include root-failed plug weld specimens, as well as toe-failed out-of-plane gusset weld joint and T-joint specimens. The welding residual stresses near the root notch and weld toe are measured by X-ray diffraction technique. The assessment of the mean stress effect on fatigue strength has been examined through the utilization of the modified MIL-HandBook-5D equivalent stress range. The equivalent stress range is evaluated by using two fatigue assessment stresses: structural stress and elastic–plastic local stress. It has been confirmed that all fatigue test results, irrespective of the failure mode or the joint type, whether from the as-welded or stress-relieved specimens, can be closely approximated using a single S–N curve with either definition of the equivalent stress. This outcome indicates the accomplishment of assessing the mean stress effect on the fatigue strength of welded joints with various failure modes and joint types.

Keywords Mean stress effect · Creep strain · Plug weld

Nomenclatures

AW	As-welded
α	Coefficient of thermal expansion or the exponent of MIL-HDBK5D equivalent stress range
β	Convective heat transfer coefficient
C_0, C_1, C_2, C_T	Material properties associated with creep
d	Distance from the root notch

$\Delta\sigma$	Nominal stress range or hot spot stress (HSS) range
$\Delta\sigma_b$	Bending components of the nominal stress range
$\Delta\sigma_m$	Membrane components of the nominal stress range
E	Young's modulus
ε^C	Creep strain
ENS	Effective notch stress
EPLSC	Elastic-plastic local stress cycle
FAT value	Fatigue strength at 2×10^6 cycles
FE	Finite element
GW	Gusset weld
HFMI	High-frequency mechanical impact
HSS	Hot spot stress
λ	Thermal conductivity
MAG	Metal active gas
MIL-HDBK	MIL-handbook
N	Number of specimens
ν	Poisson's ratio
N_f	Failure life

Recommended for publication by Commission XIII - Fatigue of Welded Components and Structures.

✉ Naoki Osawa
osawa@naoe.eng.osaka-u.ac.jp

¹ Komatsu Ltd, Hirakata, Osaka, Japan

² Department Naval Architecture and Ocean Engineering, Graduate School of Engineering, Osaka University, Suita, Osaka, Japan

³ Joining and Welding Research Institute, Osaka University, Ibaraki, Osaka, Japan

PW	Plug weld
R	Stress ratio
ρ	Density
RLS	Root local stress
$\sigma_x^{(r)}$	Normal component of WRS in the x-dir.
σ_{res}^*	Updated WRS near the hot spot
σ_{const}	Mean stress excluding WRS
σ_{max}	The maximum stress in a stress cycle
σ_{min}	The minimum stress in a stress cycle
SR	Stress relief
σ_{res}	WRS near the hot spot
Stdv	Standard deviation
σ_{VM}	Von Mises stress (in MPa)
σ_x	Stress component in x-dir.
$\bar{\sigma}_x$	Local stress in x-dir.
$\bar{\sigma}_{x,max}$	The maximum local stress in x-dir. in a stress cycle
$\bar{\sigma}_{x,min}$	The minimum local stress in x-dir. in a stress cycle
σ^Y	Yield stress
T	Temperature (in degrees Celsius)
t	Time (in seconds)
TEPFEA	Thermal elastic–plastic FE analysis
TJ	T-joint
WRS	Welding residual stress
XRD	X-ray diffraction

1 Introduction

In compact enclosed compartments of box-shaped steel structures, partial penetration welds are frequently selected as the welding technique. Root fatigue failure might manifest in these joints, and employing post-weld heat treatment (stress relief (SR)) can improve the fatigue resistance of such connections. In order to ensure the structural integrity of steel structures, it is imperative to formulate a quantitative assessment approach for evaluating the efficacy of SR treatment in enhancing the fatigue strength of root-failed welded joints. In such assessments, the mean stress effect on the fatigue strength of root-failed welded joints should be clarified. It would be of great practical value if this assessment could be performed in a uniform manner regardless of fracture type (toe failure or root failure) and joint type.

Many researchers have investigated the mean stress effect on the fatigue strength of welded joints. Baumgartner and Bruder [1] examined the fatigue strength of toe-failed longitudinal stiffeners in as-welded and SR-treated conditions and tried to transfer the fatigue test results into a single damage parameter PSWT-N curve. Hensel [2] proposed to combine cyclically stabilized local residual stress with mean stress to effective mean stress and applied the fatigue design concept based on the effective mean stress to longitudinal stiffeners.

Ahola et al. [3] and Ratfar et al. [4] performed fatigue analyses of welded joints with post-weld treatment by the 4R method, which is based on the cyclic behavior at the notch root accounting for local residual stress, and showed that the 4R method could improve the fatigue evaluation of weld root failure. However, no method has yet been established for evaluating mean stress effects on the fatigue strength of welded joints independent of fracture type and joint type.

The authors [5, 6] investigated the welding residual stress (WRS) near the root notch of plug weld (PW) specimens and carried out the fatigue tests of the as-welded (AW) and SR specimens experiencing root failure. The findings indicated that by examining the equivalent stress range derived through the modified MIL-Handbook-5D (MIL-HDBK-5D) method proposed by Matsuoka et al. [7, 8], one could predict the fatigue strength of the SR specimen subjected to cyclic loadings with arbitrary stress ratio if the fatigue strength of the AW specimen is known.

Hereafter, the stress utilized in the fatigue assessment is called “fatigue assessment stress.” Matsuoka’s method is effective when structural hot spot stress (HSS) is chosen as the fatigue assessment stress, thereby enabling the utilization of HSS S–N diagrams for a wide range of welded joints experiencing toe failure when the HSS determination technique is established [9]. An estimation technique for the mean stress effect on the fatigue strength of welded joints experiencing toe failure, regardless of the joint type, was established. However, in the case of joints experiencing root failure, it is essential to conduct fatigue tests on the as-welded specimen for each unique joint configuration since the methodology for estimating the fatigue strength of root-failed joints by using HSS S–N diagrams has not been established. It is desirable to develop an estimation technique for the mean stress effect that can be applied irrespective of the fracture mode (toe and root failure) and the joint type.

In this study, the WRS measurements in the vicinity of crack initiation sites of PW, out-of-gusset weld joint (GW), and T-joint (TJ) specimens are conducted. Bending fatigue tests are performed on these specimens. The calculation of the modified MIL-HDBK5D equivalent stress range ($\Delta\sigma_{eq}$) involves the utilization of two fatigue assessment stresses: structural stress and elastic–plastic local stress. In the former approach, HSS is employed for the toe-failed GW and TJ specimens, while the root local stress (RLS), determined by extrapolating the stress within the root gap, is employed for the root-failed PW specimen. Regarding the latter approach, the elastic–plastic local stress cycle (EPLSC), analyzed using a very fine FE mesh, is applied to both toe-failed and root-failed specimens. Based on the test results, a comprehensive evaluation is conducted to assess the effectiveness of the modified MIL-HDBK-5D method based on structural stress in relation to root-failed PW joint. Furthermore, the validity of the modified MIL-HDBK-5D method based on

EPLSC for joints experiencing both toe and root failures is examined.

2 Fatigue tests

2.1 Test specimens

In this study, WRS measurements and bending fatigue tests are carried out on PW specimens experiencing root failure, as well as GW and TJ specimens experiencing toe failure.

Figure 1 illustrates the shape and dimensions of the PW specimen. The thickness of the main plate is 16 mm, while that of the backing plate is 9 mm. The base metal is mild steel JIS: SS400, and the weld metal is JIS: YGW11. A slit is introduced at the center of the base plate and subsequently filled by MAG (100% CO₂) welding, utilizing the backing plate. The welding process comprises three consecutive passes, without any inter-pass cooling duration. The mean gap between the base metal and the backing of AW specimens is approximately 1 mm, while the average radius of the root notch measures around 0.5 mm. Those gaps and radiuses are measured by photographing the cross-sections of the specimens. PW specimen exhibits the following characteristics: (1) despite the small size of the specimen, it is capable of accommodating substantial WRS; (2) it

experiences root failure; (3) the WRS near the root notch can be measured by X-ray diffraction (XRD) method after removing/cutting backing plate. By utilizing this specimen, one can explore the correlation between WRS and the root-failure fatigue strength.

The shape and dimensions of the GW specimen are shown in Fig. 2. The base and gusset plates are mild steel JIS: SS400 with a thickness of 16 mm. The weld metal is JIS: YGW11. The mean toe radius measures approximately 0.5 mm. This specimen shows high tensile WRS along the loading axis at the weld toe and experiences toe failure.

The shape and size of the TJ specimen are presented in Fig. 3. The base and rib plates comprise a steel plate JIS: SM490A with a thickness of 19 mm. For the weld material, welding wire JIS: YGW15 is utilized. The rib is welded to the center of the base plate, measuring 500 mm × 400 mm, through the employment of MAG welding with Ar-20% CO₂ gas. Subsequently, the specimens are extracted from that joint via electrical discharge machining. The mean toe radius measures approximately 0.5 mm. This specimen experiences toe failure in fatigue tests.

The mechanical properties and the chemical components of the base and welding materials are presented in Table 1, and the welding conditions are outlined in Table 2. The mechanical properties of base and filler metals are measured by cutting a specimen from the base

Fig. 1 Plug weld (PW) specimen

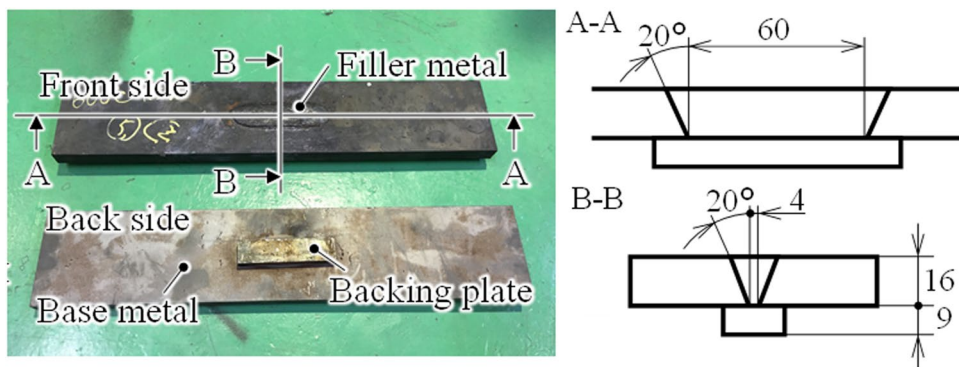


Fig. 2 Out-of-plane gusset weld (GW) specimen

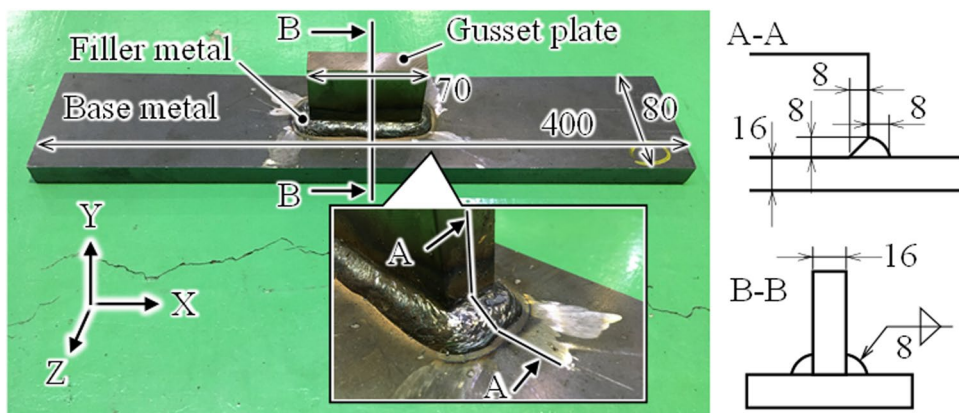


Fig. 3 T-joint (TJ) specimen

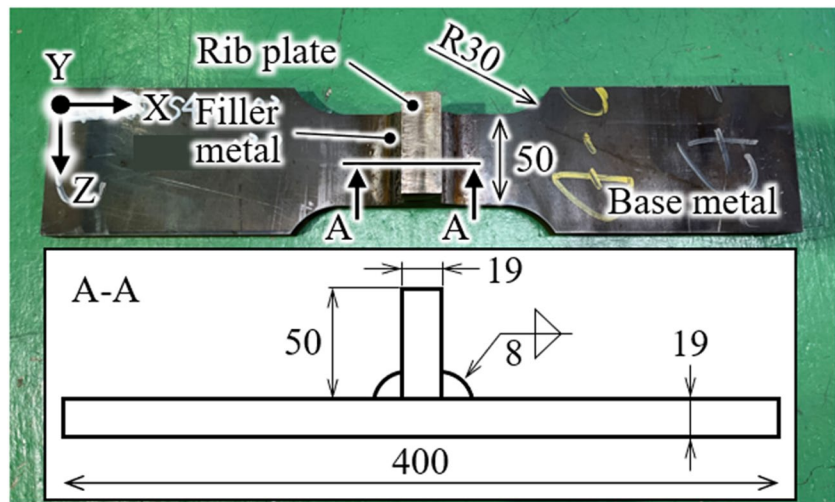


plate and weld bead of the welded joints. Alongside the as-welded (AW) specimens, stress-relieved (SR) specimens were fabricated for PW, GW, and TJ specimens, employing holding temperatures ranging from 500 to 600 °C, accompanied by holding durations of 1.5 h. Henceforth, the identifiers SR500, SR550, and SR600 are employed to refer to the SR specimen subjected to a holding temperature of 500, 550, and 600 °C.

2.2 WRS measurement

Regarding each specimen prepared in Section 2.1, the WRS in the proximity of the root notch in the PW specimen, as well as that in the vicinity of the weld toe in both the GW and TJ specimens, are measured utilizing X-ray diffraction (XRD) method [10–12]. This measurement is conducted for both the as-welded (AW) and stress-relieved (SR) specimens.

XRD measurements are performed based on the $\cos\alpha$ method [13–15] using Pulstec μ -X360s. The collimator diameter is 1 mm. The X-ray irradiation range is about 3 mm, and the distance from the toe or root notch to the nearest measurement point is 1.5 mm. The surfaces of the measurement region are smoothed by electropolishing to a metallic luster to avoid the effects of oxide scale and surface roughness.

As the weld root of the PW specimen is concealed by the backing plate, direct assessment of the WRS is unfeasible. Consequently, the overhanging section of the backing plate is removed via electrical discharge machining, as depicted in Fig. 4. The presence or absence of the excised portion minimally affects the rigidity of the region adjacent to the root notch, and the impact on WRS caused by the excision is negligible [1, 2].

2.3 Fatigue tests

In order to investigate the correlation between the WRS in the region near the root notch or the weld toe, and the fatigue strength of specimens under as-welded (AW) and stress-relieved (SR) conditions, a series of four-point bending fatigue tests are conducted. The bending fatigue tests are preferred due to the ease of controlling the local mean stress, even in the presence of welding distortion. For the cyclic loading, a Shimadzu Servo Pulser hydraulic fatigue testing machine with a capacity of 50 kN is employed. The specimen is supported by two pins at both ends, positioned at intervals of 350 mm, while two additional pins are used to drive upwards and downwards at intervals of 150 mm within the end pins, as depicted in Fig. 5. A constant amplitude fully reversed sinusoidal load with stress ratio (R) of -1 and 0 is applied at a frequency of 8 Hz.

JSSC fatigue design guideline [16] stipulates that the nominal stress range $\Delta\sigma$ used in fatigue assessment is calculated as $\Delta\sigma = \Delta\sigma_m + \gamma \Delta\sigma_b$ regardless of joint type, where $\Delta\sigma_m$ and $\Delta\sigma_b$ are membrane and bending components of the nominal stress range. The correction factor for the bending component, γ , is given to be 0.8 in the guideline. The validity of this correction under the specified test conditions ($R = -1$ and 0) is confirmed by Araki et al. [17].

2.4 Thermal elastic–plastic FE analysis (TEPFEA)

The WRS in both PW and GW specimens is examined through the utilization of thermal elastic–plastic finite element analysis (TEPFEA). The TEPFEA is carried out employing JWRIAN-ISM, an implicit TEPFEA code based on the iterative sub-structuring method developed by Murakawa et al. [18, 19]. The finite element (FE) meshes employed for the analysis are illustrated in Figs. 6 and 7.

Table 1 Mechanical properties and chemical components of specimens

(a) Mechanical properties		Grade	Yield strength (MPa)		Tensile strength (MPa)	
Specimen	Material					
PW	Base metal	SS400 (JIS G3101)	297		467	
	Backing plate	SS400 (JIS G3101)	280		452	
	Filler metal	YGW11 (JIS Z3312)	346		515	
GW	Base metal	SS400 (JIS G3101)	297		467	
	Gusset plate	SS400 (JIS G3101)	297		467	
	Filler metal	YGW11 (JIS Z3312)	409		501	
TJ	Base metal	SM490A (JIS G3106)	422		552	
	Rib plate	SM490A (JIS G3106)	422		552	
	Filler metal	YGW15 (JIS Z3312)	409		501	

(b) Chemical components		Thickness (mm)	%C	%Si	%Mn	%P	%S	%Cu	%Ni	%Cr	%No	%Nb	%V
			×100	×100	×100	×10000	×1000	×100	×100	×100	×100	×100	×100
SS400 (JIS G3101)	10	17	1	95	16	5	-	-	-	-	-	-	-
	13	17	1	95	15	6	-	-	-	-	-	-	-
	17	16	2	90	13	3	-	-	-	-	-	-	-
SM490A (JIS G3106)	19	16	3	136	13	4	1	1	3	0	1	0	0

Table 2 Welding conditions of specimens

Specimen	Bead	Current (A)	Voltage (V)	Welding speed (cpm)
PW	1st pass	300	28	45
	2nd pass	350	34	30
	3rd pass	400	38	30
GW	Fillet	250	28	30
TJ	Fillet	350	35	35

The shape of the weld bead is determined based on macroscopic observations. In the case of the PW specimen, a 1-mm gap is set between the base metal and the backing plate, while the radius of the root notch is set to 0.5 mm, as per the measurements. As for the GW specimen, the radius of the weld toe is also set to 0.5 mm, based on measurements. The minimum element edge length in the vicinity of the root notch or weld toe is set at 0.15 mm. This specific length is determined through the mesh sensitivity

analysis conducted by the authors [20]. In the welding and SR treatment analyses, rigid motion suppression boundary conditions are applied to the FE models.

Because many researchers (e.g., [21–23]) have successfully implemented the assumption of elastic perfectly plastic material model in the WRS analysis, a bilinear hardening material model with Von Mises yielding criteria and small tangent modulus is adopted in this study. Bhatti et al. [24] investigated the influence of thermo-mechanical material properties of different steel grades (S355–S960) on WRS in T-fillet joints. They concluded that the temperature dependence of yield stress has the most decisive influence on the accuracy of WRS calculations. Murakawa et al. [18, 19] optimized the temperature dependence of material properties so that the calculated AW WRS agreed with those measured for steel materials nearly identical to those used in this study.

From the above discussion, the material parameters for TEPFEA are determined by the following procedure: the

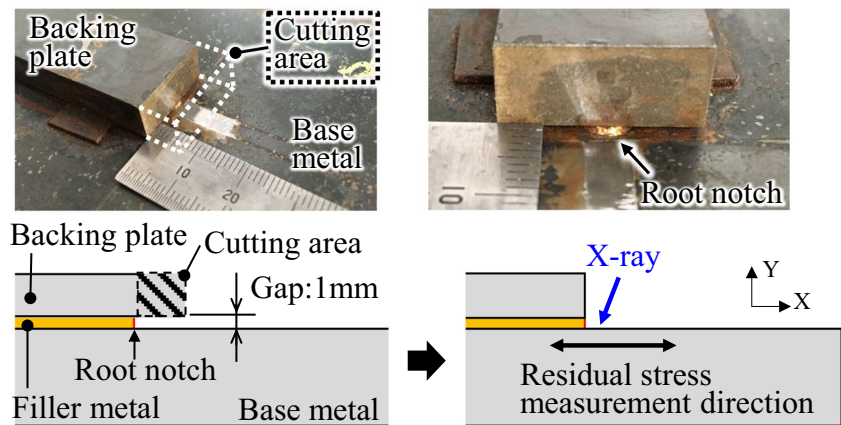
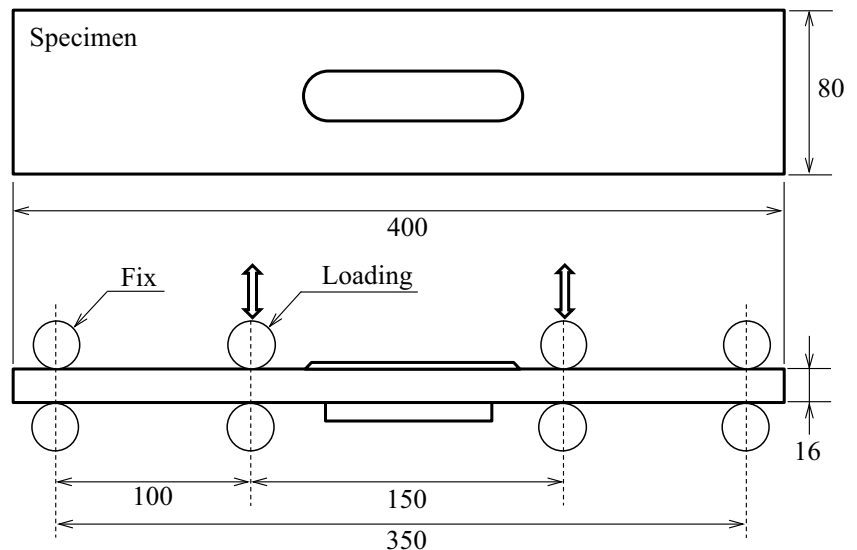
Fig. 4 WRS measurement method near the root notch**Fig. 5** Fatigue testing setup

Fig. 6 FE model of PW specimen

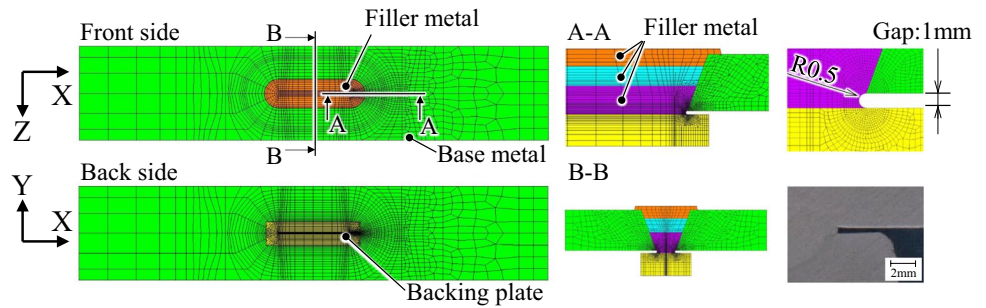


Fig. 7 FE model of GW specimen

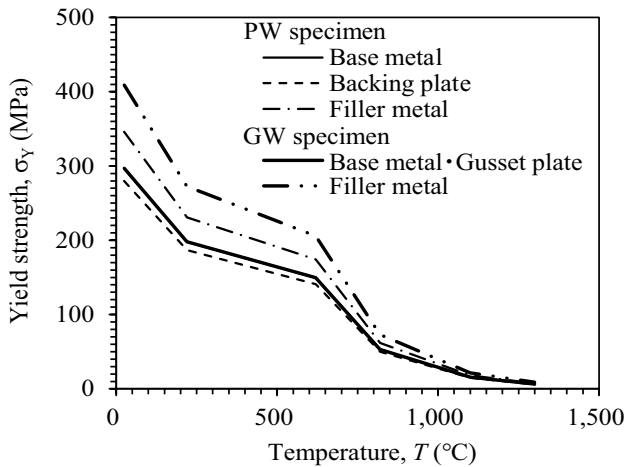
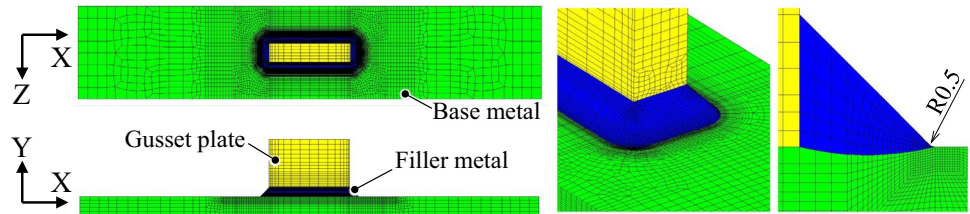


Fig. 8 Temperature dependence of yield strength

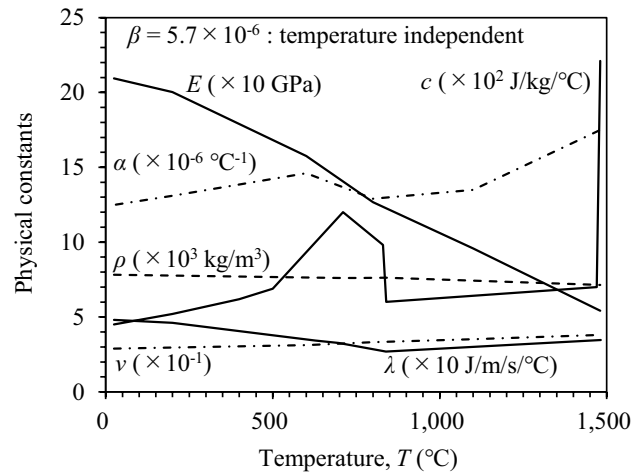


Fig. 9 Temperature dependence of physical constants

mechanical properties at room temperature are determined based on measurements conducted at room temperature (Table 1(a)); the ratio of properties at room temperature to those at elevated temperature is approximated to be the same as that those in Refs. [18, 19]; following Refs. [18, 19], the hardening coefficient h is set to 1/1000 of Young's modulus.

The yield stresses (σ^Y) of the materials used for the PW and GW specimens are assigned temperature dependency, as illustrated in Fig. 8. The temperature dependencies of specific heat (c), Young's modulus (E), coefficient of thermal expansion (α), convective heat transfer coefficient (β), thermal conductivity (λ), Poisson's ratio (ν), and density (ρ) are also considered as shown in Fig. 9.

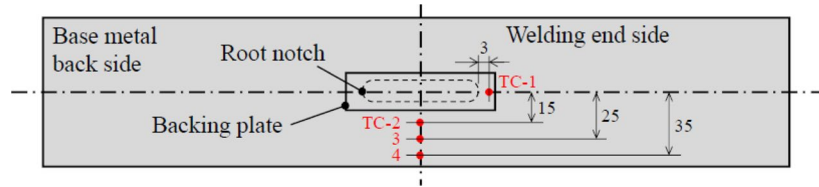
The shapes of the filler metal regions in the FE model are determined to match the measured cross-sectional shape of

the weld layer. The welding heat is applied as a moving heat source, which follows the trajectory of the welding torch. The amount of heat is determined through calculations based on the welding current, voltage, and torch speed, as provided in Table 2. The distribution of heat input is approximated by a rotating ellipsoid, where the radii differ before and after the heat source. The dimensions of the heat source and the heat input efficiency (η) are adjusted in order to achieve agreement between the calculated weld penetration shape and the measured ones. These adjusted parameters are documented in Table 3. As shown in Fig. 10a, the temperature histories in PW specimens are measured by K-type thermocouples with a wire diameter of 0.65 mm at four points (TC-1 ~4). An example of the comparison between the calculated and measured thermal cycles of a PW specimen is depicted in Fig. 10a.

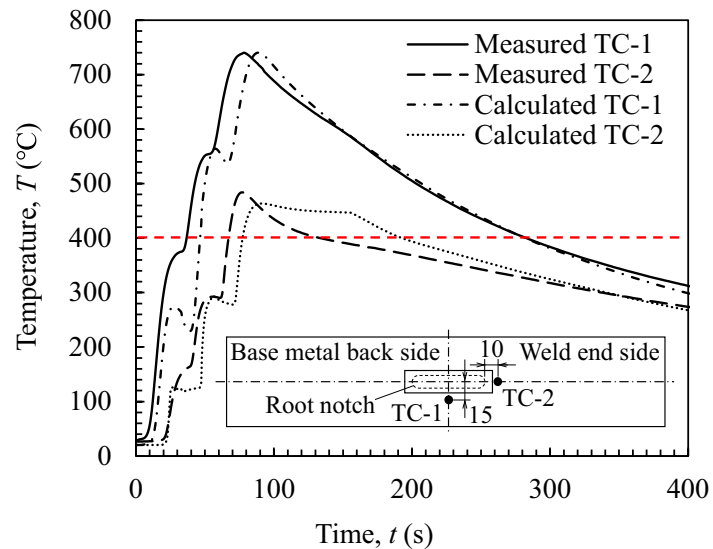
Table 3 Welding heat input parameters

Specimen	Bead	Heat source length (mm)	Heat source width (mm)	Heat source depth (mm)	Heat input efficiency η
PW	1st pass	20	12	7	0.9
	2nd pass	35	14	10	0.9
	3rd pass	35	16	15	0.9
GW	Fillet	20	13	6	0.9

Fig. 10 Thermal cycles in PW specimen during the welding process



(a) The arrangement of temperature measurement points for PW specimen



(b) Comparison of measured and calculated temperature histories

In the case of PW specimens, creep deformation is incorporated into the TEPFEA. This is due to the relatively low heat capacity of these specimens and the sustained high temperatures of 400 °C or higher in the vicinity of the weld for an extended duration. The Norton-Bailey model [25] is employed to simulate the creep deformation, and the corresponding creep strain (ϵ^C) is calculated using Eq. (1).

$$\epsilon^C = C_0 (\sigma_{VM})^{C_1} t^{C_2} \exp\left(-\frac{C_T}{\Theta}\right) \quad (1)$$

$C_1 > 1, 0 \leq C_2 \leq 1.0, ; \Theta = 273.15 + T$

where σ_{VM} is the von Mises stress (in MPa), t denotes time (in seconds), T signifies temperature (in degrees Celsius), and $C_0, C_1, C_2,$ and C_T are the material properties associated with creep. Those properties, obtained from the references [5], are presented in Table 4.

Table 4 Norton-Bailey creep model parameters (stress in MPa)

C_0	C_1	C_2	C_T
1.43E-07	1.9	0.46	2315.8

Conversely, creep is not taken into consideration for GW specimens since the elevated temperature exceeding 400 °C is of short duration.

3 Experimental and analysis results

3.1 Fatigue test results

The visual representation, fracture surface, and trajectory of fatigue crack propagation in the PW specimens are depicted

in Fig. 11. Likewise, Figs. 12 and 13 illustrate those of the GW and TJ specimens, respectively. The measurement locations for WRS in the PW and GW specimens, as detailed in Section 2.2, align with the points of crack initiation. The correlation between the nominal stress range $\Delta\sigma$ and the failure life N_f is presented in Fig. 14.

The fatigue lives of the SR600 data exhibit approximately 3.5 times greater longevity than the AW data in the PW specimens and about 2.5 times greater longevity in the GW specimens, signifying an enhancement of approximately two

and one classification grades, respectively, within the JSSC fatigue strength grade A–D. The fatigue strength at 2×10^6 cycles (FAT value) for JSSC grade A–D is 190, 155, 125, and 100 MPa.

The test data for PW specimens with $R=0$ is depicted using solid circle markers for AW and solid square markers for SR600. In these instances, the increment in fatigue strength resulting from SR in comparison to AW is marginal. The test data for TJ specimens with $R=-1$ is illustrated with open diamond markers for AW and solid diamond

Fig. 11 PW specimen after fatigue test (a appearance, b fracture surface, c crack propagation path)

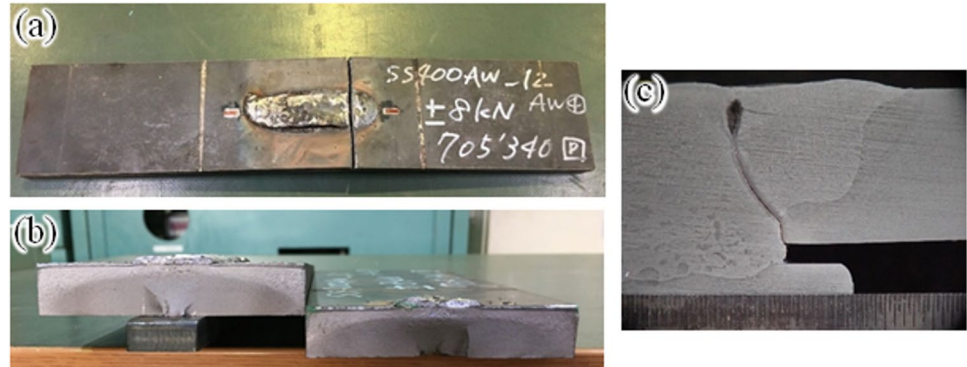
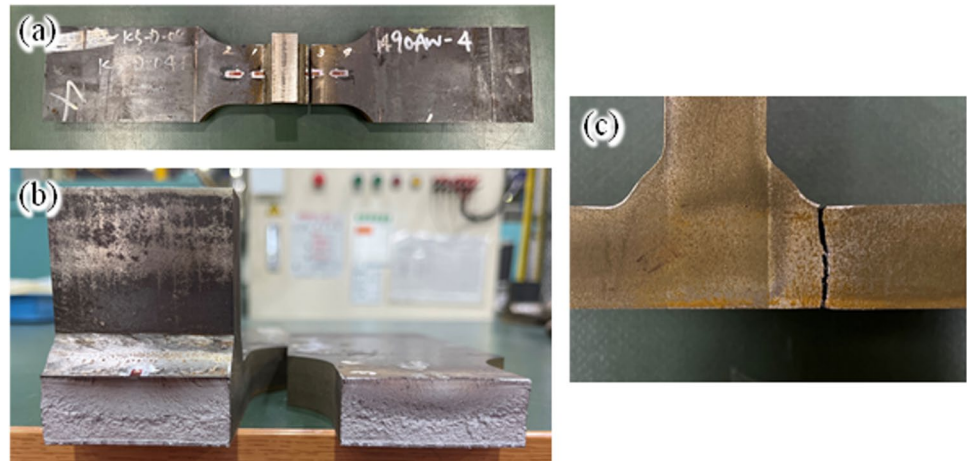


Fig. 12 GW specimen after fatigue test (a appearance, b fracture surface, c crack propagation path)



Fig. 13 TJ specimen after fatigue test (a appearance, b fracture surface, c crack propagation path)



markers for SR600. The fatigue strength of both cases is comparable.

3.2 WRS at crack initiation sites

3.2.1 Root notch in PW specimens

The X-coordinates presented in Fig. 4 are utilized in the subsequent analysis. Consider d as the distance measured along the X-axis from the root notch, and let $\sigma_x^{(r)}$ denote the normal component of WRS in the X-direction. The region where d is less than 8 mm corresponds to the interior of the root gap. Within the AW specimen, the $\sigma_x^{(r)}$ in the root gap exhibits tensile characteristics, ranging from approximately 80 to 200 MPa. Figure 15 shows $\sigma_x^{(r)}$ for the SR500 and SR600 specimens, where N is the number of test specimens with the same conditions. In this measurement, multiple specimens ($N=2$ or 3) are prepared for each SR condition. WRS is measured in all specimens, and they are plotted in Fig. 15. The significant variation in WRS measurements is caused by a combination of individual differences in the specimens and uncertainties in the XRD measurements. In this figure, the tensile $\sigma_x^{(r)}$ induced in AW specimens decreases through SR at a temperature of 500 °C for a duration of 1.5 h. Furthermore, it is observed that SR at a temperature of 600 °C for 1.5 h leads to complete relaxation of the stress (< 50 MPa). This decrease in the WRS is considered to be accountable for the enhanced root failure fatigue strength of the SR600 specimens.

3.2.2 Weld toe in GW and TJ specimens

In this subsection, d signifies the distance measured along the X-axis from the weld toe. Figure 16 exhibits the relation between $\sigma_x^{(r)}$ and d for six AW GW specimens. $\sigma_x^{(r)}$ is

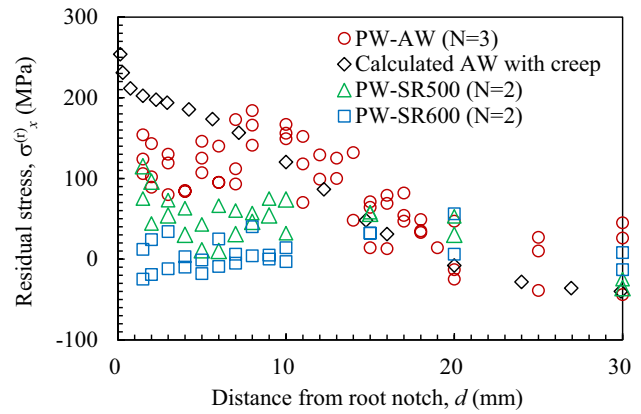
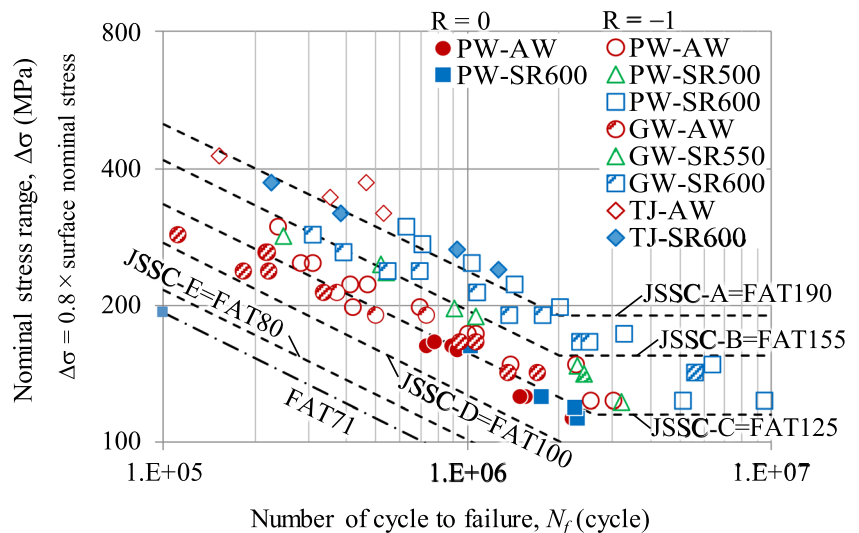


Fig. 15 Relation between WRS's X-component $\sigma_x^{(r)}$ and distance from the root notch d of PW specimens

tensile near the weld toe in AW specimens, with an average value of approximately 320 MPa at $d=1.5$ mm. $\sigma_x^{(r)}$ for SR550 (six specimens) and SR600 (three specimens) cases are also plotted in this figure. It is shown that the tensile $\sigma_x^{(r)}$ generated in AW specimens is reduced by 550 °C, 1.5 h of SR, and completely relaxed (< 50 MPa) by 600 °C, 1.5 h of SR. Similar to Fig. 15, multiple specimens ($N=3$ to 6) are prepared for each SR condition, and WRS is measured in all specimens. The significant variation in WRS measurements in Fig. 16 is caused by a combination of individual differences in the specimens and uncertainties in the XRD measurements.

$\sigma_x^{(r)}$ is measured at $d=1.5$ mm along the center line of the base metal. $\sigma_x^{(r)}$ in SR600 specimens approaches insignificance, and the disparity in WRS pre- and post-SR is negligible. The fatigue strength of AW specimens and SR600 specimens exhibit no discernible distinction.

Fig. 14 Fatigue test results of PW, GW, and TJ specimens



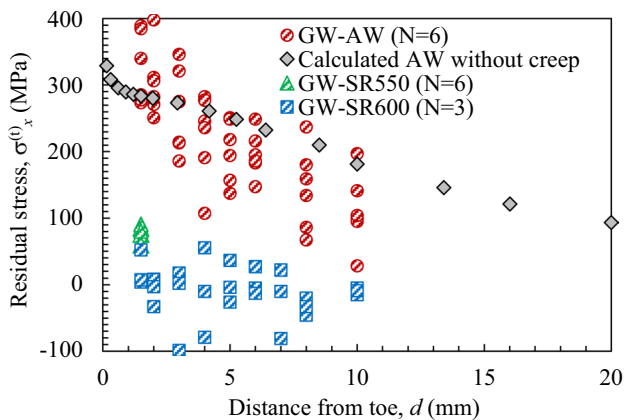


Fig. 16 Relation between WRS’s X-component $\sigma_x^{(r)}$ and distance from the toe d of GW specimens

4 Mean stress effect evaluation by hot spot stress

Matsuoka et al. [7–9] conducted an assessment of the fatigue life of weld joints that failed at the weld toe, employing the MIL-HDBK-5D method [18], which incorporates the influence of mean stress resulting from WRS. Within this methodology, the fatigue capacity is appraised using hot spot stress (HSS)-based equivalent stress range $\Delta\sigma_{eq}$ calculated by Eq. (2),

$$\Delta\sigma_{eq} = (\Delta\sigma)^\alpha \left(\frac{\Delta\sigma}{2} + \sigma_{const} + \sigma_{res} \right)^{1-\alpha}; \alpha = 0.6485 \quad (2)$$

where $\Delta\sigma$ is HSS range, σ_{const} is the mean stresses excluding WRS, and σ_{res} is the WRS near the hot spot. This formula was originally proposed in US Military Standard [26], and α is determined by the experiments [7, 8].

The localized maximum and minimum stresses, accounting for both mean stress and WRS, can be computed utilizing Eq. (2). Let $\bar{\sigma}_{max}$ and $\bar{\sigma}_{min}$ be the maximum and minimum in a stress cycle. In the event that the absolute value of either $\bar{\sigma}_{max}$ or $\bar{\sigma}_{min}$ surpasses the yield stress σ^Y , the WRS σ_{res} is updated to σ_{res}^* given by Eq. (3).

$$\sigma_{res}^* = \begin{cases} \sigma^Y - \left(\sigma_{const} + \frac{\Delta\sigma}{2} \right) & (\bar{\sigma}_{max} > \sigma^Y) \\ \sigma_{res} & (otherwise) \\ -\sigma^Y - \left(\sigma_{const} - \frac{\Delta\sigma}{2} \right) & \bar{\sigma}_{min} < -\sigma^Y \end{cases} \quad (3)$$

Subsequently, we proceed to examine the equivalent stress range given by Eq. (2) to approximate the fatigue test results through the utilization of a unified S–N diagram encompassing various joint configurations and failure modes (namely, root failure and toe failure). Equation (3) is derived by approximating that the material is elastic–fully plastic material. Matsuoka et al. [7, 8] showed

experimentally that even with this simplification, the equivalent stresses in Eq. (2) can be used to accurately estimate the mean stress effect on the fatigue strength of welded joints subject to variable amplitude loadings. In Eq. (3), the external stress is evaluated by HSS. Since the WRS is an elastic–plastic stress field and no elastic stress singularity occurs. Therefore, the stress concentrations of HSS and local WRS are comparable, and it is acceptable to use them together.

σ_{res} is derived from the XRD data obtained in the vicinity of the root notch or the weld toe. The HSS of the GW and TJ samples is determined using the elastic FEA and the IIW’s 0.4h–1.0h two-point extrapolation technique [27]. The HSS of the TJ specimen exhibits a nearly identical value to the nominal stress.

For a PW specimen, an examination is conducted on the stress distribution along the central axis of the base metal in the vicinity of the root notch using elastic FEA. The FEA results reveal that the principal direction coincides with the X-axis, which is the loading direction. The stress component σ_x exhibits an elastic singularity at $d=0$, gradually decreasing and converging towards the nominal stress as d increases. The relationship between d and σ_x , as determined through calculations, is depicted in Fig. 17.

This stress distribution bears resemblance to that observed near the gusset end of a GW specimen. Consequently, in the context of the structural stress approach, the “root local stress (RLS)” is adopted as the fatigue evaluation stress. RLS is determined by IIW’s 0.4h–1.0h two-point extrapolation method [27], which involves extrapolating the back face stress of the base metal to the root notch.

When calculating the $\Delta\sigma_{eq}$, the values of $\Delta\sigma$ and σ_{const} are obtained through the computation of HSS or RLS. These values are then multiplied by the bending correction factor $\gamma=0.8$. The resulting $\Delta\sigma_{eq}$ is presented in Table 5.

Figure 18 depicts the correlation between the structural stress-based $\Delta\sigma_{eq}$ and N_f . It is noteworthy that the AW fatigue test results with $R = -1$ for various specimen types, characterized by different joint geometries and failure modes (root failure and toe failure), can be effectively represented by a unified S–N diagram. This indicates the validity of the IIW’s extrapolation method for GW and TJ specimens, enabling the estimation of fatigue life for PW specimens experiencing root failure through the utilization of root local stress (RLS) and the HSS S–N diagram.

Figure 18 additionally illustrates the fatigue test results of SR specimens, featuring a stress ratio of $R = -1$, as well as those of PW specimens in AW and SR conditions with $R=0$. Remarkably, all test results can be effectively approximated using the same S–N diagram employed for $R = -1$.

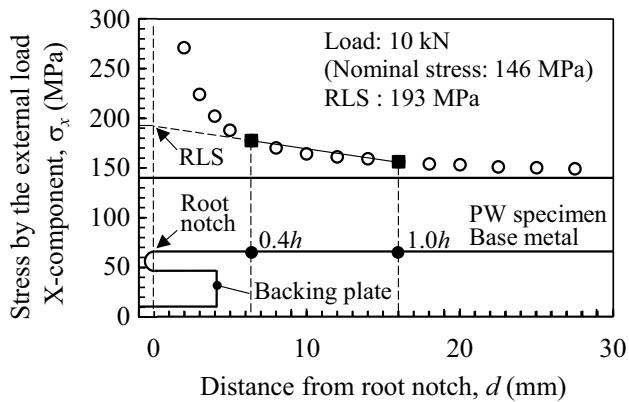


Fig. 17 Stress X-component σ_x near the root notch of PW specimen by the external load

This indicates that irrespective of variations in joint geometry and failure modes (root failure or toe failure), the MIL-HDBK-5D method is capable of quantitatively assessing the influence of mean stress caused by alterations in stress ratio (R) and/or WRS under the conditions chosen.

The results show that the mean stress effect due to the WRS relaxation caused by SR can be quantitatively evaluated.

Figures 16 and 17 demonstrate that the WRS near the root notch (for PW specimens) and the weld toe (for GW specimens) in the AW state can be reliably approximated by TEPFEA. By substituting these estimations of σ_{res} into Eqs. (2) and (3), the impact of mean stress can be evaluated without the need for XRD measurements. The mean value of WRS for the same SR condition is listed in Table 5, and it is used as σ_{res} in Eq. (2).

In the case of SR specimens, if the alteration in WRS caused by SR treatment can be precisely estimated by TEPFEA, taking into account creep phenomena, the influence of mean stress resulting from the SR treatment can be exclusively assessed through numerical simulation. This methodology proves especially advantageous for root-failed welded joints, where direct measurement of WRS poses challenges. To accomplish such an analysis, it is imperative to ascertain the creep characteristics that can replicate the creep deformations occurring during the SR process.

5 Mean stress effect evaluation by local elastic–plastic stress cycle

In Section 4, it is exemplified that the mean stress effect arising from variations in stress ratio and/or WRS can be assessed using the MIL-HDBK-5D equivalent stress range, relying on structural stress (HSS or RLS), irrespective of

disparities in joint geometry and failure modes. Nevertheless, it is postulated that the fatigue test data cannot be approximated by the integrated S–N diagram depicted in Fig. 18 when the toe profile is modified through grinding or HFMI treatment.

In the PW specimen, the structural stress (RLS) can be determined. It is deemed that this accounts for the capability to approximate the root-failed PW specimen's test result through the HSS S–N diagram. Nevertheless, in the majority of root-failed joints, the stress distribution near the root notch deviates considerably from that observed near the weld toe, where the validity of IIW's two-point extrapolation method prevails. In such instances, the evaluation of root-failed fatigue strength becomes unattainable through the HSS S–N diagram. The regressed S–N curve with a slope of 4.049 is plotted in this figure. The Stdv of $\log(N_f)$ is fairly small at 0.033.

Let “elastic–plastic local stress cycle (EPLSC)” denote the localized stress cycle at the crack initiation site, specifically the weld toe or root notch. This cycle is determined by employing a fine FE mesh that accurately replicates the local profile of either the weld toe or the root notch. The calculation of EPLSC involves welding TEPFEA, followed by a cyclic elastic–plastic FE analysis (EPFEA). In this analysis, the WRS in the AW condition and its relaxation during fatigue loading are thoroughly investigated. The analysis of EPLSC can be applied to any root-failed welded joint with arbitrary root geometry. It is anticipated that the fatigue test results can be approximated using a unified S–N diagram, regardless of joint geometry and failure mode, by evaluating the MIL-HDBK-5D equivalent stress $\Delta\sigma_{eq}$ derived from the EPLSC. This fatigue assessment approach is referred to as the “EPLSC method.”

In the EPLSC method, the mesh sensitivity of the local stress converges at a relatively coarse mesh size due to the occurrence of plastic deformation and the elimination of elastic stress singularity. Consequently, the EPLSC method obviates the necessity of incorporating artificial notch geometries, as is required by the effective notch stress (ENS) approach [28].

In this chapter, the determination of $\Delta\sigma_{eq}$ using the EPLSC method is carried out for both PW and GW specimens, followed by an examination of the relationship between $\Delta\sigma_{eq}$ and N_f . The FE mesh presented in Figs. 6 and 7, as employed in the TEPFEA outlined in Section 2.4, serves as the model for the cyclic EPFEA. The minimum element edge length is 0.15 mm. The mesh sensitivity of EPLSC converges at this particular mesh size, under the conditions chosen. The cyclic loading analysis is conducted as a restart analysis from the AW condition, wherein a constant amplitude four-point bending load is applied, with a nominal stress range $\Delta\sigma$ and a stress ratio

Table 5 Fatigue test results and stress assessment methods

Specimen	SR		Yield σ_Y (MPa)	WRS σ_{res} (MPa)	Load		Nominal stress				RLS or HSS			MIL-HDBK-5D		EPLSC				N_f (cycle)	Crack initiation		
	Temp (°C)	Hold (h)			P_{max} (kN)	P_{min} (kN)	σ_{max} (MPa)	σ_{min} (MPa)	$\Delta\sigma$ (MPa)	$0.8 \cdot \Delta\sigma$ (MPa)	σ_{min} (MPa)	σ_{max} (MPa)	$0.8 \cdot \Delta\sigma$ (MPa)	σ_{res}^* (MPa)	$\Delta\sigma_{eq}$ (MPa)	σ_{max} (MPa)	σ_{min} (MPa)	$\Delta\sigma$ (MPa)	$\Delta\sigma_{eq}$ (MPa)				
PW R=0	AW-1	—	—	297	128	12.75	0.5	187	7	179	144	246	10	213	89	239	551	-92	643	609	892,603	root	
	AW-2	—	—	297	128	12.75	0.5	187	7	179	144	246	10	213	89	239	551	-92	643	609	741,857	root	
	AW-3	—	—	297	128	10	0.5	146	7	139	111	193	10	165	128	201	512	-33	545	533	1,558,551	root	
	AW-4	—	—	297	128	10	0.5	146	7	139	111	193	10	165	128	201	512	-33	545	533	1,504,187	root	
	AW-5	—	—	297	128	9	0.5	132	7	125	100	174	10	147	128	184	499	35	463	476	2,221,577	root	
	AW-6	—	—	297	128	13	0.5	190	7	183	146	251	10	217	84	242	554	-102	656	618	784,426	root	
	AW-7	—	—	297	128	12.5	0.5	183	7	176	141	241	10	208	93	236	544	-87	631	599	933,614	root	
	SR600-1	600	1.5	297	44	12.75	0.5	187	7	179	144	246	10	213	44	226	—	—	—	—	—	1,034,659	root
	SR600-2	600	1.5	297	44	9	0.5	132	7	125	100	174	10	147	44	162	—	—	—	—	—	2,325,261	root
	SR600-3	600	1.5	297	44	10	0.5	146	7	139	111	193	10	165	44	179	—	—	—	—	—	1,769,619	root
SR600-4	600	1.5	297	44	9.5	0.5	139	7	132	105	183	10	156	44	170	—	—	—	—	—	2,280,339	root	
PW R=1	AW-1	—	—	297	128	6	-6	92	-92	184	148	116	-116	185	128	197	467	-375	842	684	2,291,783	root	
	AW-2	—	—	297	128	5	-5	77	-77	154	123	96	-96	154	128	170	452	-270	722	613	2,561,350	root	
	AW-3	—	—	297	128	7	-7	108	-108	215	172	135	-135	216	128	223	481	-436	916	731	1,013,290	root	
	AW-4	—	—	297	128	8	-8	123	-123	246	197	154	-154	247	128	248	495	-483	979	770	705,340	root	
	AW-5	—	—	297	128	9	-9	138	-138	277	221	174	-174	278	128	274	509	-522	1,031	805	476,088	root	
	AW-6	—	—	297	128	8	-8	123	-123	246	197	154	-154	247	128	248	495	-483	979	770	424,086	root	
	AW-7	—	—	297	128	6	-6	92	-92	184	148	116	-116	185	128	197	467	-375	842	684	1,400,982	root	
	AW-8	—	—	297	128	10	-10	154	-154	307	246	193	-193	308	128	299	523	-554	1,077	835	314,223	root	
	AW-9	—	—	297	128	5	-5	77	-77	154	123	96	-96	154	128	170	452	-270	722	613	3,050,030	root	
	AW-10	—	—	297	128	9	-9	138	-138	277	221	174	-174	278	128	274	509	-522	1,031	805	414,207	root	
	AW-11	—	—	297	128	7	-7	108	-108	215	172	135	-135	216	128	223	481	-436	916	731	1,071,019	root	
	AW-12	—	—	297	128	10	-10	154	-154	307	246	193	-193	308	128	299	523	-554	1,077	835	286,688	root	
	AW-13	—	—	297	128	12	-12	184	-184	369	295	231	-231	370	112	343	551	-603	1,154	890	241,211	root	
	SR500-1	500	1.5	297	95	10	-10	154	-154	307	246	193	-193	308	95	286	—	—	—	—	—	519,474	root
	SR500-2	500	1.5	297	95	6	-6	92	-92	184	148	116	-116	185	95	186	—	—	—	—	—	2,296,755	root
	SR500-3	500	1.5	297	95	8	-8	123	-123	246	197	154	-154	247	95	236	—	—	—	—	—	905,716	root
	SR500-4	500	1.5	297	95	5	-5	77	-77	154	123	96	-96	154	95	160	—	—	—	—	—	3,223,671	root
	SR600-1	600	1.5	297	0	6	-6	92	-92	184	148	116	-116	185	0	145	—	—	—	—	—	6,488,426	root
	SR600-2	600	1.5	297	0	5	-5	77	-77	154	123	96	-96	154	0	121	—	—	—	—	—	5,159,724	root
	SR600-3	600	1.5	297	0	7	-7	108	-108	215	172	135	-135	216	0	169	—	—	—	—	—	3,314,805	root
	SR600-4	600	1.5	297	0	8	-8	123	-123	246	197	154	-154	247	0	193	—	—	—	—	—	2,045,019	root
	SR600-5	600	1.5	297	0	9	-9	138	-138	277	221	174	-174	278	0	218	—	—	—	—	—	1,440,675	root
	SR600-6	600	1.5	297	0	10	-10	154	-154	307	246	193	-193	308	0	242	—	—	—	—	—	1,044,354	root
	SR600-7	600	1.5	297	0	5	-5	77	-77	154	123	96	-96	154	0	121	—	—	—	—	—	9,566,632	root
	SR600-8	600	1.5	297	0	12	-12	184	-184	369	295	231	-231	370	0	290	—	—	—	—	—	633,684	root
	SR600-9	600	1.5	297	0	11	-11	169	-169	338	271	212	-212	339	0	266	—	—	—	—	—	714,964	root
	GW R=1	AW-1	—	—	297	325	9	-9	133	-133	266	213	167	-167	267	164	277	521	-415	937	762	374,719	toe
		AW-2	—	—	297	325	11	-11	162	-162	325	260	204	-204	326	134	315	544	-492	1,036	826	220,653	toe
		AW-3	—	—	297	325	7	-7	103	-103	207	165	130	-130	207	193	235	498	-217	714	629	1,073,074	toe
		AW-4	—	—	297	325	8	-8	118	-118	236	189	148	-148	237	179	257	509	-317	826	697	743,183	toe
		AW-5	—	—	297	325	10	-10	148	-148	295	236	185	-185	296	149	296	533	-460	993	798	184,161	toe
		AW-6	—	—	297	325	6	-6	89	-89	177	142	111	-111	178	208	213	487	-117	604	560	1,371,328	toe
		AW-7	—	—	297	325	12	-12	177	-177	354	283	222	-222	355	119	334	556	-523	1,079	855	112,885	toe
AW-8		—	—	297	325	10	-10	148	-148	295	236	185	-185	296	149	296	533	-460	993	798	223,207	toe	
AW-9		—	—	297	325	8	-8	118	-118	236	189	148	-148	237	179	257	509	-317	826	697	502,704	toe	
AW-10		—	—	297	325	6	-6	89	-89	177	142	111	-111	178	208	213	487	-117	604	560	1,706,344	toe	
AW-11		—	—	297	325	11	-11	162	-162	325	260	204	-204	326	134	315	544	-492	1,036	826	222,879	toe	
AW-12		—	—	297	325	9	-9	133	-133	266	213	167	-167	267	164	277	521	-415	937	762	338,043	toe	
AW-13		—	—	297	325	7	-7	103	-103	207	165	130	-130	207	193	235	498	-217	714	629	952,978	toe	
SR550-1		550	1.5	297	80	10	-10	148	-148	295	236	185	-185	296	80	270	—	—	—	—	—	540,663	toe
SR550-2		550	1.5	297	80	12	-12	177	-177	354	283	222	-222	355	80	317	—	—	—	—	—	247,210	toe
SR550-3		550	1.5	297	80	6	-6	89	-89	177	142	111	-111	178	80	175	—	—	—	—	—	2,407,026	toe
SR550-4		550	1.5	297	80	8	-8	118	-118	236	189	148	-148	237	80	223	—	—	—	—	—	1,069,243	toe
SR600-1		600	1.5	297	21	9	-9	133	-133	266	213	167	-167	267	21	220	—	—	—	—	—	1,083,052	toe
SR600-2		600	1.5	297	21	7	-7	103	-103	207	165	130	-130	207	21	173	—	—	—	—	—	2,381,658	toe
SR600-3		600	1.5	297	21	8	-8	118	-118	236	189	148	-148	237	21	197	—	—	—	—	—	1,791,595	toe
SR600-4		600	1.5	297	21	6	-6	89	-89	177	142	111	-111	178	21	150	—	—	—	—	—	5,653,579	toe
SR600-5																							

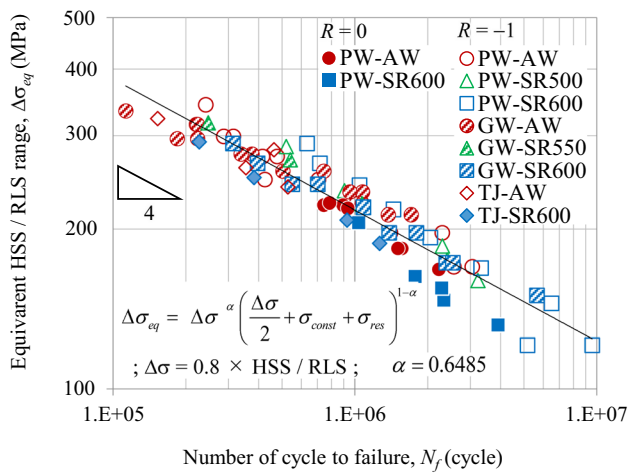


Fig. 18 The relation between failure lives N_f and modified MIL-HDBK-5D equivalent stress ranges $\Delta\sigma_{eq}$ for cases with various specimens and WRS

of $R=0$. In these scenarios, the maximum nominal stress experienced, σ_{max} , is given by $\sigma_{max} = \Delta\sigma$. The number of loading cycles is three.

Figure 19 illustrates the computed EPLSC, specifically referring to the local stress in the x -direction ($\bar{\sigma}_x$), at the point of crack initiation (the root notch for PW specimens, weld toe for GW specimens). Subsequently, Fig. 20 depicts the distributions of $\bar{\sigma}_x$ at two distinct instances: the as-welded (AW) condition and the end of the initial load cycle, both in proximity to the crack initiation sites.

In Fig. 19, the relaxation of the WRS takes place during the initial loading cycle, leading to an alteration in the WRS distribution as depicted in Fig. 20. However, this alteration almost converges after the second cycle.

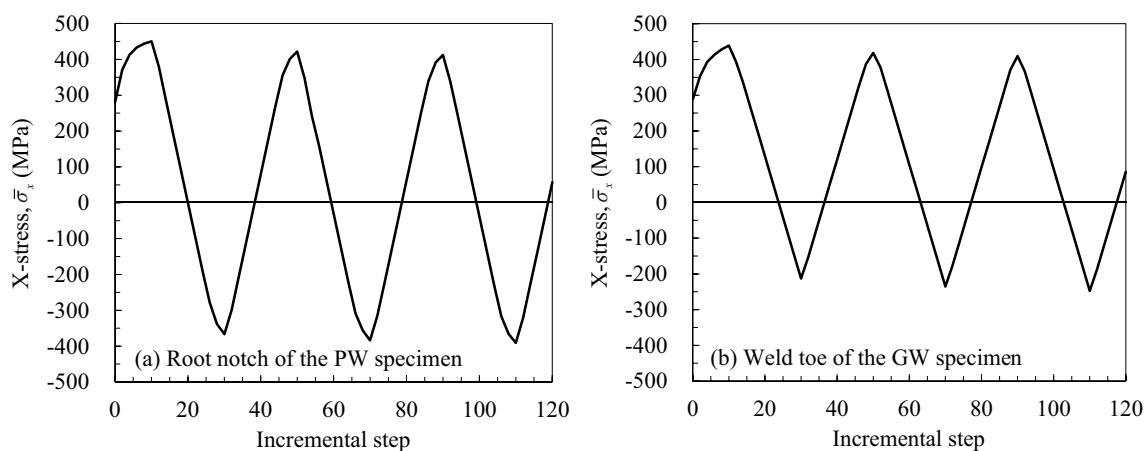


Fig. 19 The calculated time histories of $\bar{\sigma}_x$ at the root notch of the PW specimen and that at the weld toe of the GW specimen subject to the cyclic loadings with the load amplitude of ΔP_{max} ($R = -1$)

Based on these findings, the EPLSC is evaluated from the time history of $\bar{\sigma}_x$ in the third cycle for each loading condition.

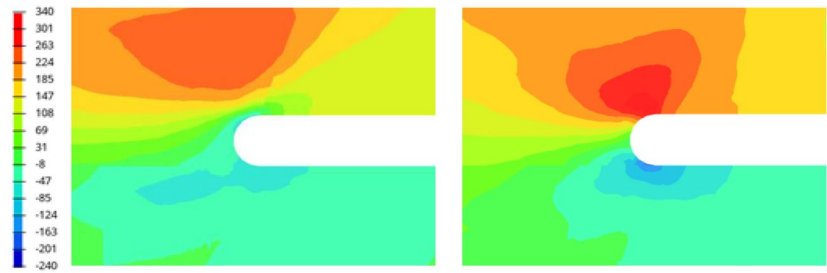
The EPLSC is determined for each loading condition of the fatigue tests conducted on the PW and GW specimens, employing the aforementioned procedure. For each condition, the equivalent stress ($\Delta\sigma_{eq}$) is computed from the maximum and minimum $\bar{\sigma}_x$ observed in the EPLSC, utilizing Eq. (4). The utilization of the bending correction factor γ mentioned in Section 4 is not employed since the change in the stress gradient in the direction of thickness, as a result of bending loading, is inherently considered in the EPFEA with a very fine FE mesh.

$$\Delta\sigma_{eq} = (\Delta\bar{\sigma}_x)^\alpha (\bar{\sigma}_{x,max})^{1-\alpha}; \Delta\bar{\sigma}_x = \bar{\sigma}_{x,max} - \bar{\sigma}_{x,min}, \alpha = 0.6485 \quad (4)$$

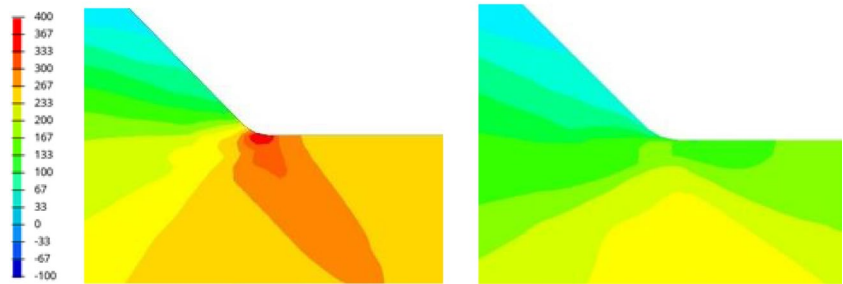
where, $\bar{\sigma}_{x,max}$ and $\bar{\sigma}_{x,min}$ are the maximum and minimum $\bar{\sigma}_x$ in a stress cycle. The difference in equivalent stress ($\Delta\sigma_{eq}$) calculated using Eq. (4) from the EPLSC in the AW fatigue tests of the PW and GW specimens is presented in Table 5. The correlation between $\Delta\sigma_{eq}$ and N_f is depicted in Fig. 21. The regressed S–N curve with a slope of 5.917 is plotted in this figure. The Stdv of $\log(N_f)$ is fairly small at 0.020. Remarkably, irrespective of variations in joint geometry, failure modes, stress ratio (R), and the WRS employed, the relationship between $\Delta\sigma_{eq}$ and N_f can be approximated by a single S–N diagram, analogous to Fig. 18. This outcome demonstrates the validity of the EPLSC-based mean stress effect evaluation for the AW specimens with differences in joint geometry and failure modes under the conditions chosen.

Once the creep characteristics of the material are established, it becomes feasible to assess the impact of stress relief (SR) on the enhancement of fatigue strength

Fig. 20 The distributions of $\bar{\sigma}_x$ near the root notch the PW specimen and that near the weld toe of the GW specimen in AW condition and at the end of the 1st loading cycle ($R = -1$; unit, MPa)



i) AW
ii) The end of the 1st cycle
(a) Root notch of the PW specimen.



i) AW
ii) The end of the 1st cycle
(b) Weld toe of the GW specimen.

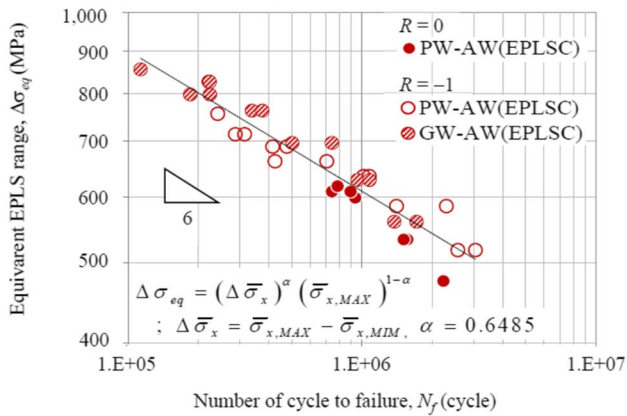


Fig. 21 The relation between failure lives N_f and modified MIL-HDBK-5D equivalent stress ranges $\Delta\sigma_{eq}$ estimated from the calculated elastic–plastic local stress cycles

through the EPLSC method. Moreover, the application of the EPLSC method can be extended to evaluate the fatigue strength improvement resulting from variations in the toe profile and the compressive WRS induced by high-frequency mechanical impact (HFMI). The comprehensive validation of these analyses will be the focal point of future investigations.

6 Conclusions

The measurement of the welding residual stress (WRS) in the vicinity of crack initiation sites of specimens with different types of joints, such as plug weld (PW), out-of-gusset weld (GW), and T-joint (TJ) specimens, is conducted. Bending fatigue tests are performed on these joint specimens. The calculation of the modified MIL-HDBK5D equivalent stress range ($\Delta\sigma_{eq}$) involves the utilization of two fatigue assessment stresses: structural stress and elastic–plastic local stress. In the former approach, the structural hot spot stress (HSS) is employed for the toe-failed GW and TJ specimens, while the root local stress (RLS), determined by extrapolating the stress within the root gap, is employed for the root-failed PW specimen. Regarding the latter approach, the elastic–plastic local stress cycle (EPLSC), analyzed using a very fine FE mesh, is applied to both toe-failed and root-failed specimens. Based on the test results, a comprehensive evaluation is conducted to assess the effectiveness of the modified MIL-HDBK-5D method based on structural stress in relation to root-failed PW joint. Furthermore, the validity of the modified MIL-HDBK-5D method based on EPLSC for various joints experiencing both toe and root failures is examined.

The findings of this study can be summarized as follows:

- (1) Under the conditions chosen, all fatigue test results can be approximated by a unified S–N diagram regardless of the joint type, failure mode, and stress ratio when the fatigue assessment stress is evaluated by the $\Delta\sigma_{eq}$ based on structural HSS (for toe-failed joints) or RLS (for root-failed joints). The Stdv of $\log(N_f)$ is fairly small at 0.033.
- (2) Under the conditions chosen, fatigue test results of PW and GW specimens in AW condition with a stress ratio of $R \leq 0$ can be approximated by a unified S–N diagram regardless of the joint type, failure mode, and stress ratio $R \leq 0$ when the fatigue assessment stress is evaluated by the $\Delta\sigma_{eq}$ based on EPLSC. The Stdv of $\log(N_f)$ is fairly small at 0.020.

The aforementioned findings indicate that the modified MIL-HDBK-5D methodology can accomplish an assessment of the influence of mean stress on weld fatigue, regardless of the geometry of the joint and the mode of failure.

Acknowledgements This study was conducted as a part of the Osaka University-Komatsu joint research project. Dr. Norio Yamamoto of Nippon Kaiji Kyokai gave us valuable advice and discussions on the application of the modified MIL-HDBK-5D method. Mr. Taiyo Kagase, of Osaka University, gave us great help in TEPFEA. At the end of this paper, I would like to express our deepest gratitude to all concerned.

Funding Open Access funding provided by Osaka University.

Data availability The data that support the findings of this study are available from the corresponding author, N.O., upon reasonable request.

Declarations

Conflict of interest The authors declare no competing interests.

Open Access This article is licensed under a Creative Commons Attribution 4.0 International License, which permits use, sharing, adaptation, distribution and reproduction in any medium or format, as long as you give appropriate credit to the original author(s) and the source, provide a link to the Creative Commons licence, and indicate if changes were made. The images or other third party material in this article are included in the article's Creative Commons licence, unless indicated otherwise in a credit line to the material. If material is not included in the article's Creative Commons licence and your intended use is not permitted by statutory regulation or exceeds the permitted use, you will need to obtain permission directly from the copyright holder. To view a copy of this licence, visit <http://creativecommons.org/licenses/by/4.0/>.

References

1. Baumgartner J, Bruder T (2013) Influence of weld geometry and residual stresses on the fatigue strength of longitudinal stiffeners. *Weld World* 57:841–855
2. Hensel J (2020) Mean stress correction in fatigue design under consideration of welding residual stress. *Weld World* 64:535–544
3. Ahola A, Muikku A, Braun M, Björk T (2021) Fatigue strength assessment of ground fillet-welded joints using 4R method. *Int J Fatigue* 142:105916
4. Raftar HR, Dabiri E, Ahola A, Björk T (2022) Weld root fatigue assessment of load-carrying fillet welded joints: 4R method compared to other methods. *Int J Fatigue* 156:106623
5. Yoshihara Y, Osawa N, and Murakawa H (2022) Study on the relationship between root-failure fatigue strength and root welding residual stress of plug welded specimens, IIW Doc. XIII-2954–2022
6. Yoshihara Y, Osawa N, and Murakawa H (2022) Numerical and experimental evaluation on residual stress related to fatigue life at the weld root of plug joint, Proceedings of IIW2022 International Conference:454–457
7. Matsuoka K, Fujii E (1995) An evaluation method on fatigue crack initiation life at welded joints in steel structures. *J Soc Naval Archi Japan* 178:513–522 ((in Japanese))
8. Yamamoto N, Matsuoka K (2001) (2001) Fatigue assessment method considering an effect of mean stress. *J Soc Naval Archi Japan* 190:499–505 ((in Japanese))
9. Yamamoto N (2017) Fatigue evaluation of ship structures considering change in mean stress condition. *Weld World* 61:987–995
10. Macherauch E, Muller P (1958) Evaluation of X-ray elastic constants of cold-strained Armco-iron and CrMo-steel. *Arch Eisenhüttenwes* 29:257–260
11. Macherauch E (1963) Principles and problems of the X-ray determination of elastic stresses. *Materialpruefung* 5:14–25
12. The Society of Materials Science Japan (2002) Standard for X-ray stress measurement iron and steel, JSMS-SD-5–02 (in Japanese)
13. He BB (2009) Two-dimensional X-ray diffraction. John Wiley & Sons
14. Yoshioka Y, Hasegawa K, Mochiki K (1978) Application of position sensitive proportional counter to X-ray stress measurement. *J Soc Mater Sci Japan* 27(294):216–220 ((in Japanese))
15. Tanaka K (2017) X-ray stress measurement by the $\cos\alpha$ method using two-dimensional detector Part2: Measurement procedure and applications. *J Soc Mater Sci Japan* 66(7):479–487 ((in Japanese))
16. Japanese Society of Steel Construction (2012) Fatigue design recommendations for steel structures, Gihodo (in Japanese)
17. Araki A, Mori T (2009) Fatigue strength of non-load carrying type cruciform welded joints subjected to plate bending and axial forces, Proceedings of 64th Annual Academic Meeting of Japan Society of Civil Engineers, 01–0162 (in Japanese)
18. Murakawa H, Ma N, Huang H (2014) Iterative substructure method employing concept of inherent strain for large-scale welding problems. *Weld World* 59:53–63
19. Nishikawa H, Serizawa H, Murakawa H (2007) Actual application of FEM to analysis of large scale mechanical problems in welding. *Sci Technol Weld Join* 12–2:147–152
20. Peiyuan D, Kyaw PM, Osawa N, Rashed S, Ma D, Okada J, Honnami M (2023) Numerical study on local residual stresses induced by high frequency mechanical impact post-weld treatment using the optimized displacement-controlled simulation method. *J Manufact Process* 92:262–271
21. Liang W, Murakawa H (2012) An inverse analysis method to estimate inherent deformations in thin plate welded joints. *Mater Des* 40:190–198
22. Canas J, Picon R, Paris F, Blazquez A, Marin JC (1996) A simplified numerical analysis of residual stresses in aluminum welded plates. *Comput Struct* 58(1):59–69
23. Deng D, Liang W, Murakawa H (2007) Determination of welding deformation in fillet welded joint by means of numerical simulation and comparison with experimental measurements. *J Mater Process Technol* 183(2–3):219–225

24. Bhatti AB, Barsoum Z, Murakawa H, Barsoum I (2015) Influence of thermo-mechanical material properties of different steel grades on welding residual stresses and angular distortion. *Mater Des* 65:878–889
25. Odquis F, Hult J (1962) *Kriechfestigkeit metallischer Werkstoffe*. Springer-Verlag, Berlin (**in German**)
26. US Military Standard (1983) MIL-HDBK-5D I, pp.16–18
27. Hobbacher, A (2008) IIW fatigue recommendations, IIW-1823–07
28. Fricke, W. (2006) IW recommendations for the fatigue assessment of welded structures by notch stress analysis, IIW-2006–09

Publisher's Note Springer Nature remains neutral with regard to jurisdictional claims in published maps and institutional affiliations.